Poly(ethylene imine) and Tetraethylenepentamine as Protecting Agents for Metallic Copper Nanoparticles

Petri Pulkkinen,[†] Jun Shan,[†] Kirsi Leppänen,[‡] Ari Känsäkoski,[§] Ari Laiho,[⊥] Mikael Järn,[¶] and Heikki Tenhu*[,†]

Laboratory of Polymer Chemistry, University of Helsinki, Helsinki, Finland, Division of Materials Physics, University of Helsinki, Helsinki, Finland, Oy Keskuslaboratorio - Centrallaboratorium Ab, Espoo, Finland, Laboratory of Optics and Molecular Materials, Helsinki University of Technology, Helsinki, Finland, and Department of Physical Chemistry, Åbo Akademi University, Turku, Finland

ABSTRACT The aim of this research was to explore the use of amine-containing polymeric and low-molar-mass organic protecting agents in the preparation of copper nanoparticles. Particles were synthesized using poly(ethylene imine) (PEI) or tetraethylenepentamine (TEPA) as protecting agents. The resulting particles were studied with UV−vis spectrometry, thermogravimetry, scanning electron microscopy, and transmission electron microscopy, wide-angle X-ray scattering with heating, X-ray photoelectron spectroscopy, and Auger electron spectroscopy. The average crystal sizes for the particles were at room temperature 8.5 and 19.4 nm for PEI and TEPA, respectively, and some surface oxidation was observed. The particles were sintered on paper, and the resistance and resistivity were measured. For Cu/PEI samples, the protecting agent was removed upon sintering at relatively low temperatures (between 150 and 200 °C). At this temperature range, particles exhibited a rapid increase in the crystal size. Sintered particles exhibited high conductivity, indicating that these kinds of materials might find use in paper-based printing.

KEYWORDS: copper nanoparticles • amine-protected nanoparticles • sintering • conductivity

INTRODUCTION

Modern society is heavily dependent on conducting materials from which various electrical applications can be fabricated. New applications are being designed, and often the new designs and methods require new materials. Interest toward modern nanoscale metal particles has received a large amount of attention lately because they offer promising alternatives for traditional methods. Nanoparticles offer easy processibility because they have lower melting points than bulk metals and interesting optical, electronic, and magnetic properties. Easy deposition methods are available to nanoparticles, and conductive inks have been synthesized (1−3). Nanoparticle materials gain conductive properties via sintering, during which the particles adhere to each other to form a conductive stain.

Copper particles are found to aggregate severely without proper protection. Further, copper nanoparticles oxidize easily in air. Recent studies (4) show that copper nanoparticles are, at room temperature, only oxidized from the surface. Although gold and silver withstand oxidation better than copper, copper is still a very attractive candidate for future conducting materials because of its abundance and cheapness. The problems of aggregation and oxidation can be circumvented by the use of various protecting agents such as polymers (5, 6) and organic ligands (3). Also, copper has been found to form various copper sulfides when reacted with sulfur-containing compounds (7−9). The interesting feature of these sulfides is the fact that they are semiconductors and quite resistant to oxidation in air. However, the conductivity of sulfides is not as good as that of pure metallic particles. Despite the interesting properties and advantages of the nanosized metal particles, the means to produce minimally oxidized copper nanoparticles in the water phase still remains a challenge.

Many difficulties introduced by the solution reduction method can be avoided by using methods such as chemical vapor deposition, laser ablation, and sputtering deposition. Recently, Luechinger et al. synthesized air-stable, ink-jet-capable, graphene-stabilized copper nanoparticles by using reducing flame synthesis (10, 11). However, these kinds of strategies require special equipment, which is not required by simple solution reduction methods.

Gold (12−14), silver (1), and copper (6, 15−25) particles have been considerably studied. Various ways to synthesize copper particles in solution exist in the literature: poly(vinylpyrrolidone) (PVP) and ascorbic acid have been used by Wu et al. (15) and Wang et al. (16). Park et al. (2) describe a way to synthesize a copper-based ink using PVP and sodium phosphinate monohydrate. Khanna et al. (17) employed

* E-mail: heikki.tenhu@helsinki.fi.
Received for review November 14, 2008 and accepted January 2, 2009
[†] Laboratory of Polymer Chemistry, University of Helsinki.
[‡] Division of Materials Physics, University of Helsinki.
[§] Oy Keskuslaboratorio - Centrallaboratorium Ab.
[⊥] Helsinki University of Technology.
[¶] Åbo Akademi University.
DOI: 10.1021/am800177d

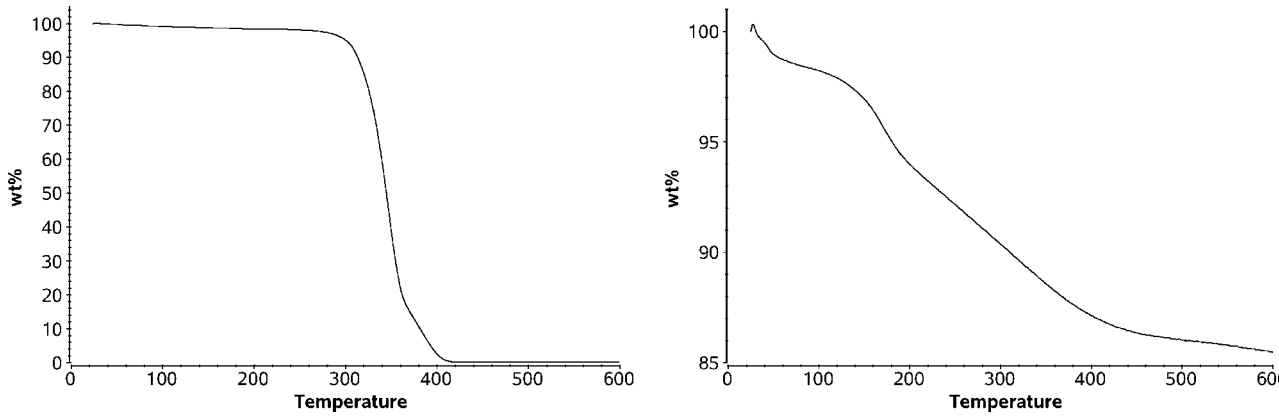

FIGURE 1. TGA data: pure PEI, left; Cu/PEI, right.

Table 1. Sintering of Cu/PEI under Various Conditions and Corresponding Resistances for 4 and 24 h Reactions

temperature/°C	force/kN	time/s	resistance (4 h)/Ω	resistance (24 h)/Ω
150	8.5	30	10^6	
200	8	15	1−3	
200	8.5	60	1−3	$(10-400) \times 10^6$
200	20	30	1−3	
250	8.5	30	<1	$(3-10) \times 10^6$

Table 2. Sintering of Cu/TEPA under Various Conditions and Corresponding Resistances

temperature/°C	force/kN	time/s	resistance/Ω
150	9.0	30	1−2
200	8.5	30	1
250	8.0	30	0.5−1

different carboxylic acids and poly(vinyl alcohol). Kanninnen et al. (18) studied lauric acid, alkanethiols of various sizes, and oleic acid to protect the copper. Mott et al. (3) reduced copper acetylacetonate with 1,2-hexadecanethiol and protected the particles with oleic acid and oleylamine. Lisiecki et al. (19) reduced copper dodecyl sulfate with sodium borohydride, and Qi et al. (20) reduced copper in various water-in-oil microemulsions. Song et al. (21) used bis(ethylhexyl)hydrogen phosphate to protect copper. Salzemann et al. (22) used copper(II) bis(2-ethylhexyl)sulfosuccinate as a copper source. Altogether, a vast range of compounds, both polymeric and small molecules, have been used to synthesize nanoscale copper structures. Compounds containing amine groups, for example, poly(ethylene imine) (PEI), have not received very much attention so far. However, the ability of amine groups to complex with the copper ions makes these compounds attractive for the preparation and subsequent protection of copper nanoparticles. The advantage of using amine-containing protecting agents is the fact that, upon pyrolysis or sintering, metallic copper is formed, not copper sulfide, as when the particles are protected with sulfur-containing moieties (8).

This study focuses on water-phase-synthesized metallic copper nanoparticles protected with amine-containing polymeric and oligomeric compounds, namely, on PEI and tetraethylenepentamine protected copper nanoparticles. The molar mass of the protecting agent is critical for the properties like sinterability of the nanoparticles. Thus, two compounds of very different molar masses were used. The particles were sintered on a paper substrate to produce a conducting layer of metallic copper.

EXPERIMENTAL SECTION

The following procedures were used in the particle synthesis. $CuCl_2$ was reduced to metallic copper in the presence of various additives. Particles were then purified to remove residues of the reducing agent and excess protecting agent. The product particles were sintered under various conditions to get a conductive layer pressed on the paper.

Materials and Methods. Poly(ethylene imine) (PEI; 99%) used was branched, containing primary, secondary, and tertiary amine groups in approximately a 25:50:25 ratio, with M_w = 1200. The polymer was obtained from Polysciences, Inc. Tetraethylenepentamine (TEPA; technical, 85%) and sodium borohydride ($NaBH_4$; 98.5%) were purchased from Sigma-Aldrich. Anhydrous copper(II) chloride (98%) was obtained from BDH, London. Water used in the syntheses was purified with a Purelab ultrapurification system; otherwise, distilled water was used. All reagents were used as received and degassed as described below. The sintering of the particles was performed under an ambient atmosphere using a simple press. Various temperatures, pressing forces, and pressing times were used.

Cu/PEI. In a typical synthesis, 2.4 g (2 mmol) of PEI_{1200} was dissolved in 150 mL of H_2O. A total of 269 mg (2 mmol) of $CuCl_2$ and 757 mg (20 mmol) of $NaBH_4$ were weighed in septum-sealed vials. The solution, vials, and a small amount of water were carefully degassed with nitrogen for about 30 min. A total of 5 mL of degassed solvent was used to transfer copper chloride into the polymer solution in a reaction flask, producing an intense blue color due to complexation of the copper and the polymer. Sodium borohydride dissolved in 5 mL of degassed water was added dropwise into the reaction flask. The reaction mixture turned in 4 h to a pitch-black liquid, which was washed under nitrogen with degassed water until the supernatant was neutral. Separation of the particles was performed using a centrifuge. Two batches of particles were prepared. The first with a 4 h reaction, and the other with a 24 h reaction. The yields for both syntheses were close to 60%.

Cu/TEPA. TEPA was another candidate to protect copper. The Cu/TEPA ratio used was 1:10. The synthesis procedure was as follows. A total of 946.5 mg (5 mmol) of TEPA was dissolved in 36 mL of water and degassed. A total of 189 mg (5 mmol) of $NaBH_4$ and 67 mg (0.5 mmol) of $CuCl_2$ were degassed separately. After thorough degassing, $CuCl_2$ was dissolved in 2 mL of degassed water and injected into aqueous TEPA in the reaction flask. An intensely colored complex formed immedi-

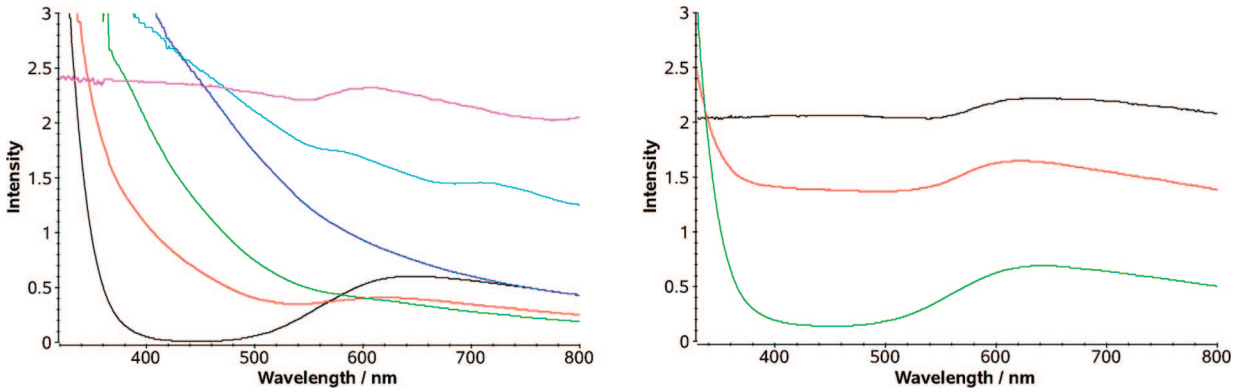

FIGURE 2. Cu/PEI UV−vis measurement. Left: no $NaBH_4$ addition (black) and 30 min (red), 1 h (green), 2 h (blue), 2 h 30 min (cyan), and 3 h (magenta) after $NaBH_4$ addition. Right: overnight (black) and 30 min (red) and 3 h 30 min (green) after opening the septum.

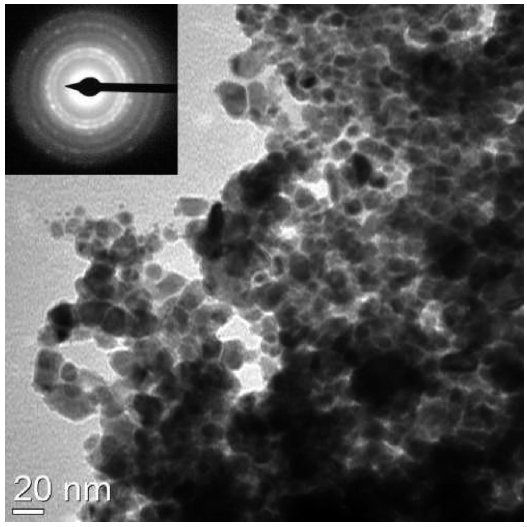

FIGURE 3. Cu/PEI TEM image of the final product.

ately. $NaBH_4$ was also transferred with 2 mL of degassed water to the reaction vessel. Quick transformation to a darker color was observed. Within 4 h, the solution turned clear, as a copper-colored precipitate formed in the flask. Purification was done under nitrogen. Precipitated particles were washed with water until the supernatant was neutral. Cu/TEPA particles were also synthesized with a 1:20 Cu/TEPA ratio with similar reaction conditions. Unless otherwise stated, 1:10 Cu/TEPA samples are described in this text. The yields for both syntheses were close to 70%.

Characterization. Thermogravimetry (TGA) measurements were done under a flowing nitrogen atmosphere using Mettler-Toledo TGA850 equipment with *STARe* software. The temperature range was 25−600 °C. Scanning electron microscopy (SEM) measurements were performed with a Hitachi S4800 field-emission scanning electron microscope. UV−vis measurements were performed with a Shimadzu UV-1601PC spectrometer. For transmission electron microscopy (TEM), the Cu/PEI solutions were drop-cast onto carbon-coated TEM grids. Cu/TEPA samples were first embedded into epoxy, and after curing of the epoxy at room temperature, thin sections (70 nm thick) were sectioned from the epoxy block onto a water surface with an ultramicrotome (Leica). Finally the thin sections were collected onto copper TEM grids followed by bright-field TEM on a FEI Tecnai 12 transmission electron microscope.

The material was also subjected to wide-angle X-ray scattering (WAXS) studies, using a small-angle X-ray scattering device specially modified for WAXS use. WAXS studies were performed using a conventional sealed X-ray tube with a copper anode and point focus. The beam was monochromatized with a nickel filter and a totally reflecting glass plate to obtain Cu Kα radiation (wavelength = 1.542 Å). The beam size used was about 1 mm × 1 mm. The sample powders were placed in 1-mm-thick aluminum rings covered with Kapton films, and measurements were carried out using perpendicular transmission geometry. An MAR345 image plate was used as the detector. The samples were heated under a helium atmosphere with a Linkam heating stage. Before each measurement, the temperature was stabilized for 10 min. The temperature was increased with a heating rate of 10 °C/min. Samples were measured for 15 min at each temperature within a range from room temperature to 350 °C. Then, the samples were cooled to room temperature. Absorption and geometrical corrections were done for the intensities. The angular range was calibrated with silver behenate and silicon, and the instrumental broadening was determined to be 0.23° at 47°. The average size of the crystallites was determined using the Scherrer formula (26).

The X-ray photoelectron spectroscopy (XPS) and Auger electron spectroscopy (AES) measurements were performed with a Physical Electronics Quantum 2000 instrument equipped with a monochromatic Al Kα X-ray source. An operating power of 25 W was used with a spot diameter of 100 μm. An electron flood gun and a low-energy ion gun were used for charge compensation. The detector position was at an angle of 45° in relation to the sample surface. The low and high resolutions of the pass energy in spectral acquisition were 117.4 and 23.5 eV, respectively. Surface concentrations were determined with *Multipak 6.1* software using peak areas to give surface concentrations in atomic percent. The binding energies were referenced to that of the adventitious carbon 1s peak at 284.6 eV. In argon ion sputtering, a focused beam with a current of 50 μA, a raster area of 2 × 2 mm^2, an acceleration voltage of 4 kV, and a sputtering time of 15 s was employed.

The resistance measurements for the sintered layer were performed using a resistance meter. Resistivity values were obtained by first measuring the dimensions and thickness of the sintered layer. The thickness was obtained from cross-sectional SEM images. The resistivity was calculated using the equation $\rho = RA/l$, where ρ is the resistivity, R the electrical resistivity, A the cross-sectional area of the sample, and l the length of the sample. For each sample, five different measurements and calculations were performed, and the average of these results was used.

RESULTS AND DISCUSSION

Cu/PEI. The synthesis procedure yielded dark particles with a metallic copper appearance. Particles sintered on paper exhibited good conducting capabilities with resistance values of less than 1 Ω at best. Details of the sintering of the particles, i.e., the temperature, applied force, and sintering

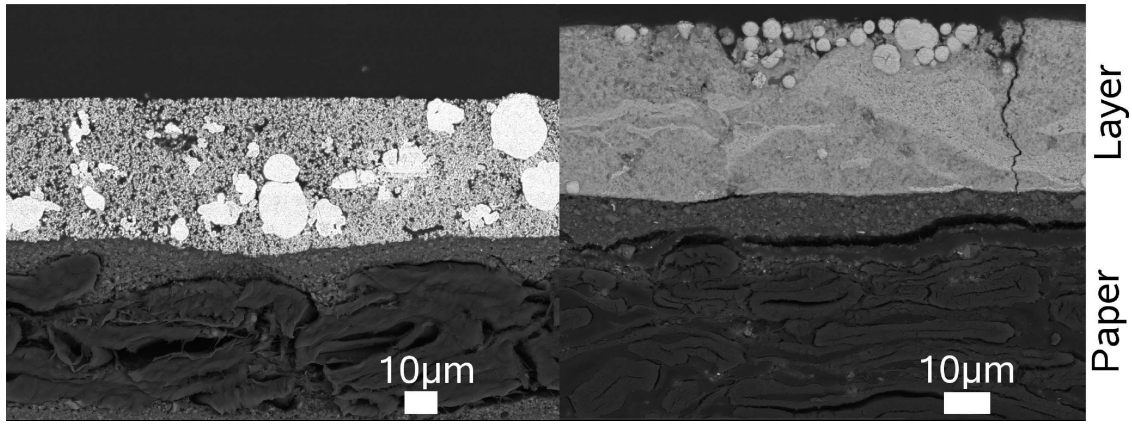

FIGURE 4. Sintered samples. Left: Cu/TEPA. Right: Cu/PEI.

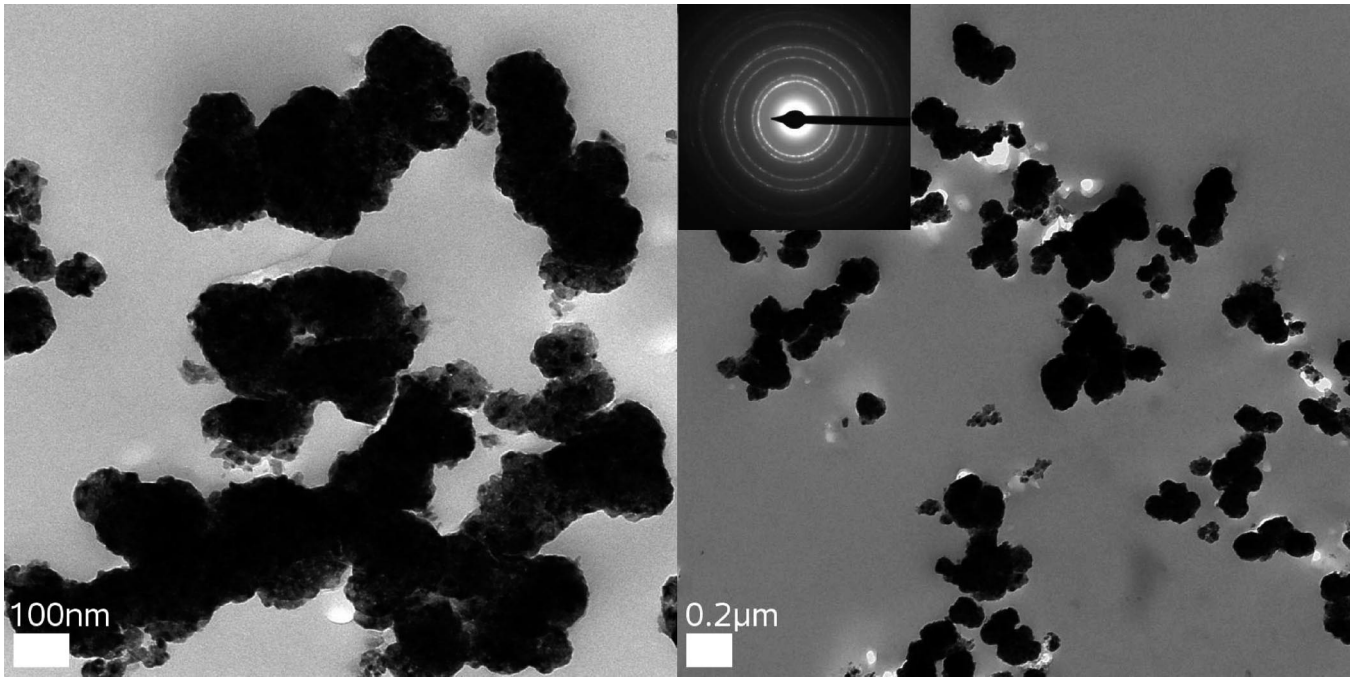

FIGURE 5. Cu/TEPA TEM images of the final product.

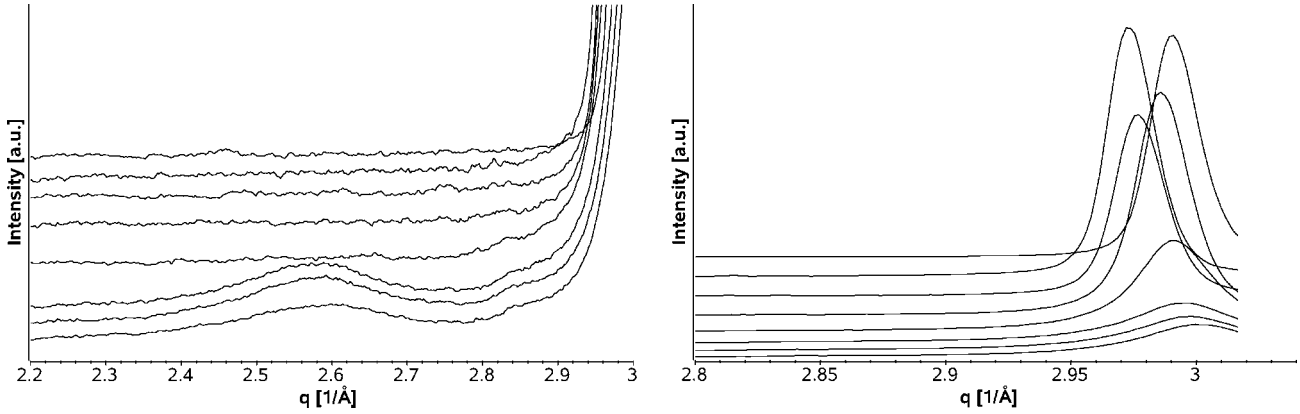

FIGURE 6. Cu/PEI WAXS recorded during heating. Left: copper oxide region. Right: metallic copper region. From the bottom line upward: 30, 100, 150, 200, 250, and 300 °C and cooled to room temperature. The spectra have been offset vertically for clarity.

time, are shown in Table 1, including also the resistances of the obtained layer. The resistance decreased greatly when 150 °C was exceeded. It was observed that the 4 h reaction yielded a product with far better conductivity than the 24 h synthesis (see Table 1), probably because of the increased interparticle aggregation with increased synthesis time. It is well-known that the melting points of nanoparticles are significantly lower than that of bulk metal (27). The heat of fusion is also lower because of the higher surface to volume ratio, which means higher amounts of defects in the crystal-

Table 3. Cu/PEI and Cu/TEPA Crystal Sizes As Measured by WAXS

	crystal size/nm		
temperature/°C	Cu/PEI	Cu/TEPA (1:10)	Cu/TEPA (1:20)
30	8.5 ± 0.3	19.4 ± 0.5	12.8 ± 0.4
100	9.4 ± 0.3	19.0	14.2 ± 0.5
150	9.9 ± 0.3	19.6	15.0 ± 0.6
200	20.0 ± 1.0	19.8	17.5 ± 0.9
250	30.0*	20.2	19.9 ± 1.2
300	*	20.8	23.8 ± 1.8
350	*	21.1	24.3 ± 1.9

line structure. Upon heating, these irregularities are repaired, increasing the crystallinity of the material. During the sintering process, the protecting agent is removed, allowing contact between the particles, resulting in the crystals growing and forming a continuous layer. According to TGA measurements, the products contained 12−15 wt % of volatile components, regardless of the reaction time. This indicates that longer synthesis times will not increase the amount of protecting agent left on the particle. TGA data also show that the nanoparticle-bound protecting agent is decomposed at lower temperature than the free PEI (see Figure 1). This probably has important consequences concerning the further processability of the protected particles. Oxides of copper are known to catalyze the decomposition of various polymers by forming an effective oxidation/reduction couple. The TGA result is in agreement with this literature data (28, 29). Also, copper oxides are known to be reduced to metallic copper when polymers are pyrolyzed in their presence (30). This may have an interesting effect on the formed conducting layer upon sintering because the protecting agent not only is removed but facilitates further reduction to metallic copper.

The samples were purified until the supernatant was neutral. During the purification, some amount of copper-colored particles precipitated on the centrifuge tube surface. This effect was especially strong when the pH of the supernatant was approaching a neutral value. This is probably due to the loss of the protecting agent during purification, causing unprotected particles to aggregate and precipitate. This is a clear indication of the relatively weak force that attaches the amine group to the metallic copper particle.

Cu/TEPA. The synthesis procedure for Cu/TEPA particles is much simpler than that for Cu/PEI particles because the product particles are easily precipitated. The resistance values of the TEPA samples are shown in Table 2. The sintering conditions have a minimal effect on the resistance values. TGA measurements indicated a very small amount of protecting agent present in the final product, only 1 % of volatile components.

UV−Vis Spectrometry. The reaction of copper in the presence of PEI was monitored with a UV−vis spectrometer. A downscaled reaction was performed in a septum-sealed quartz cuvette under nitrogen. The spectra are shown in Figure 2. Upon the addition of $NaBH_4$, a quick increase in the absorbance at low wavelengths occurs and the absorbance of the Cu/polymer complex (centered at 650 nm) diminishes. Turbidity increases rapidly, with this affecting the intensity baseline. A surface plasmon resonance peak emerges at 590 nm. The reaction was allowed to proceed overnight under nitrogen. Then, the cap was opened and the oxidation of the black liquid was monitored with time. Within 4 h, the solution turned blue and the absorbance pattern remained as the initial one, before $NaBH_4$ addition. After several days in air, the spectrum of the solution was identical with that of the initial solution with no added $NaBH_4$.

Electron Microscopy. SEM and TEM measurements were conducted on Cu/PEI samples. The purified Cu/PEI sample seemed to consist of large copper aggregates. TEM imaging, however, revealed that the large copper chunks are aggregates of finer particles (Figure 3). For the purified sample, electron diffraction showed a definite diffraction pattern because of the high amount of metallic copper present in the sample. Cross sections of the particles sintered on paper are shown for both PEI and TEPA samples in Figure 4. Both samples seem to consist of small particles fused together, forming a continuous layer. Aggregates of several micrometer size are present in the sintered layer, breaking the continuity of the layer and therefore weakening the conductivity properties. TEPA contains larger chunks than PEI and the aggregates present in the PEI sample. The large particles in Cu/TEPA are arbitrarily located in the sintered layer, suggesting that they are present in the source particles used in the sintering. This is in agreement with the large particles seen in TEM images of the Cu/TEPA particles. In the case of Cu/PEI, the large particles seem to be almost exclusively positioned on the copper−air interface, indicating that they may have formed during sintering because of contact of the layer to the pressing device or air.

TEM measurements were also performed for the Cu/TEPA samples: fine-structured aggregates of some hundred nanometers were observed before the sintering (Figure 5). The electron diffraction image gives a brighter diffraction pattern, compared to that of PEI, indicating larger particles.

WAXS Measurements. The results for Cu/PEI are presented in Figure 6. Some oxidation was observed: a crystalline Cu_2O signal can be seen (theoretically at 2.59, 2.83, and 2.96 $Å^{-1}$). A metallic copper 111 diffraction is seen as a strong peak around 3 $Å^{-1}$. During the heating experiment, the crystalline Cu_2O signal disappears. The broadness of the signal of metallic copper decreases, suggesting crystal size growth. Table 3 shows the average sizes of the metallic copper crystals calculated using Scherrer's equation for both PEI and TEPA (various ratios) samples. Above 200 °C, the crystal size starts to increase rapidly. Above 250 °C, the crystal size increases above the accurate evaluation range (marked with asterisks in the table). Evidently, this explains the increased conductivity gained by sintering because the nanocrystals fuse together at this temperature range.

The results for the Cu/TEPA particles are shown in Figure 7. No signals are observed at $q > 2.5$ $Å^{-1}$, with this indicating the absence of crystalline oxide. The heating experiment

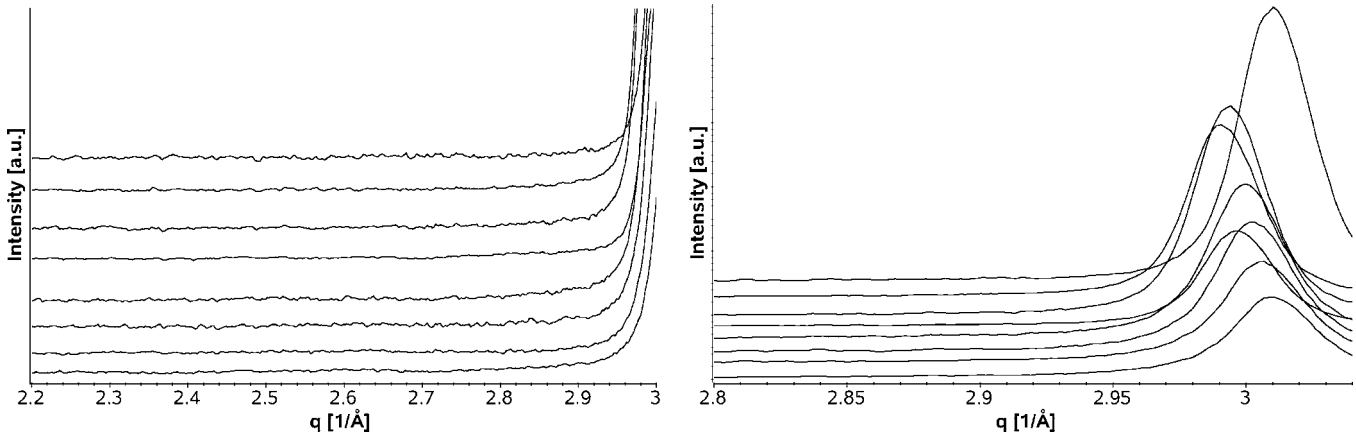

FIGURE 7. Cu/TEPA WAXS recorded during heating. Left: copper oxide region. Right: metallic copper region. From the bottom line upward: 30, 100, 150, 200, 250, and 300 °C and cooled to room temperature. The spectra have been vertically offset for clarity.

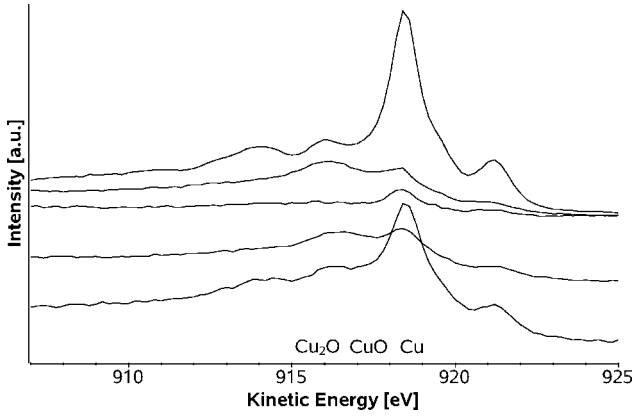

FIGURE 8. CuL_3VV Auger electron spectra. From top to bottom: copper reference, Cu/PEI, Cu/PEI sputtered, Cu/TEPA, and Cu/TEPA sputtered. The positions of Cu, Cu_2O, and CuO characteristic values (31) are marked on the image.

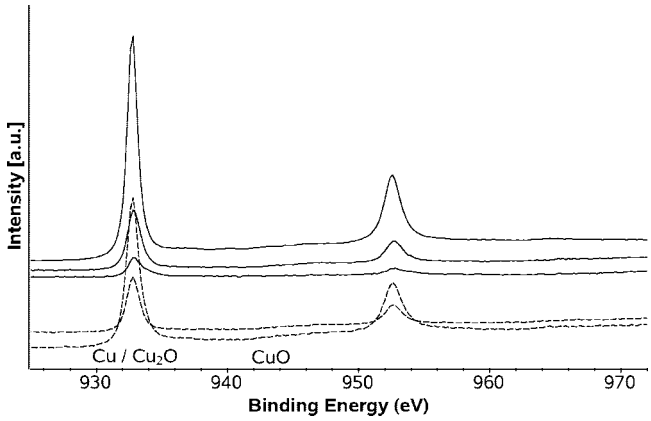

FIGURE 9. Cu 2p photoelectron spectra. From top to bottom: copper reference, Cu/PEI, Cu/PEI sputtered, Cu/TEPA, and Cu/TEPA sputtered. The positions of Cu, Cu_2O, and CuO characteristic values (31) are marked on the image.

does not show significant narrowing of the metallic copper signals, suggesting that no dramatic change in the crystal size occurs. Table 3 shows the calculated crystal sizes: apparently, the TEPA (1:10) particles do not fuse together, as the ones prepared using PEI do. Probably the crystals are too large for the temperature range used. In addition, the observed decrease of the thermal stability of the surface-bound PEI may play a role in the successful sintering of

Table 4. Cu/PEI and Cu/TEPA Compared Resistivity Results

sample	temperature/°C	force/kN	time/s	resistivity/Ω m
Cu/PEI	200	10	5	8.45×10^{-5}
Cu/PEI	200	8	30	4.14×10^{-5}
Cu/PEI	200	8.5	60	2.44×10^{-5}
Cu/PEI	200	8	15	1.11×10^{-4}
Cu/PEI	250	8.5	30	1.31×10^{-4}
Cu/TEPA	150	30	30	2.61×10^{-5}
Cu/TEPA	150	30	10	3.30×10^{-5}
Cu/TEPA	200	47	30	7.19×10^{-6}
Cu/TEPA	220	47	30	3.09×10^{-6}
Cu/TEPA	220	47	10	3.05×10^{-5}
Cu/TEPA	250	47	<1	7.81×10^{-6}

polymer-protected particles. The slight change in the crystal size can be attributed to the thermal expansion of the material. Increasing the copper/protecting agent ratio in the synthesis to 1:20 yields smaller particles, as shown in Table 3. For the smaller particles, the heating experiment causes crystals to fuse together, but not as effectively as in the case of Cu/PEI particles.

XPS and AES Measurements. CuL_3VV Auger electron spectra and Cu 2p photoelectron spectra of Cu/PEI and Cu/TEPA are shown in Figures 8 and 9, respectively. The following conclusions can be made: (i) No strong satellite peak in the Cu 2p signal characteristic of CuO (at 940−945 eV) is observed for any of the samples. (ii) Cu_2O (signal at 916 eV) is dominant in Cu/PEI and high in Cu/TEPA. (iii) Both of the sputtered samples look very similar to the reference copper. Therefore, it may be concluded that the particles are oxidized to Cu_2O from the surface, with CuO contamination being very slight. The inner part of the particle, exposed by the sputtering, is metallic copper.

Resistivity. The resistivities for sintered PEI and TEPA particles are shown in Table 4. The particles were applied on paper and pressed, varying the temperature, force, and pressing time. Cu/PEI and Cu/TEPA particles pressed on paper show resistivity values on the order of 10^{-4} and 10^{-6} Ω m, respectively, higher than that of bulk metallic copper (10^{-8} Ω m). In light of the data discussed above, the observed values may be rationalized as follows: Cu/PEI

particles are smaller and have higher surface to volume ratios than Cu/TEPA. This results in easier PEI particle oxidation, as seen in WAXS and XPS/AES data. Partly oxidized and small PEI particles are easily sintered, as shown by WAXS and resistance measurements, resulting in a continuous sintered layer. Resistivity values are decreased by the continuity of the sintered layer but also, on the other hand, are weakened by the degree of oxidation. TEPA particles show only a small increase of the crystal size upon heating, suggesting such a large average crystal size that no crystal merging occurs at the temperature range used. While no crystal merging takes place during sintering, the interparticle spacing is still low enough to form a conducting layer. Higher surface to volume ratios result in slower oxidation than that in PEI particles, as seen in WAXS and XPS/AES.

CONCLUSIONS

Both PEI and TEPA enable the preparation of copper nanomaterials with varying degrees of conductive properties. The protecting agents cover the growing nanoparticles and prevent them from coalescing. The ability of TEPA and PEI to complex copper ions slows the reduction and aggregation of the metallic copper particles, producing nanoparticle aggregates coated with the protecting agent. Upon purification, both the reducing agent and part of the protecting agent are removed, TEPA almost completely. PEI samples lose some of the protecting agent. WAXS measurement indicates that PEI- and TEPA-protected particles have average crystal sizes of 8 and 19 nm, respectively. The spacing between the nanostructures and the continuity of the conduction layer dictates the overall conductivity. In the case of Cu/PEI, the protecting agent is decomposed close to 200 °C, removing the barrier between the individual nanoparticles. Nanoparticles come into contact with each other, with this allowing them to fuse together, seen as an increase in the crystal size. A continuous conductive layer is formed, with this abruptly improving the conductivity. The thermal decomposition of the polymer may also facilitate the reduction of copper oxides into metallic copper, a phenomenon that may explain the disappearance of the copper oxide signal at 2.6 $Å^{-1}$ seen in the WAXS studies. This may also be due to the crystalline copper oxide transforming into an amorphous one.

The conductivity is not as high for Cu/PEI, as it is in the case of Cu/TEPA samples, probably because of polymer residues and oxidation of copper in the Cu/PEI sample. The observed low thermal stability of PEI bound to metal particles opens up interesting possiblities of further development of the materials. Cu/TEPA particles, according to WAXS studies, do not show an increase in the crystal size, indicating that crystals do not fuse together. The nonpolymeric protecting agent is almost completely removed from the material, and because there are no barriers preventing particles from making contact, a conductive layer is formed.

Acknowledgment. Oy Keskuslaboratorio - Centrallaboratorium Ab and the Finnish Funding Agency for Technology and Innovation are thanked for funding this project.

REFERENCES AND NOTES

(1) Lee, H. H.; Chou, K. S.; Huang, K. *Nanotechnology* **2005**, *16*, 2436–2441.
(2) Park, B. K.; Kim, D.; Jeong, S.; Moon, J.; Kim, J. S. *Thin Solid Films* **2007**, *515*, 7706–7711.
(3) Mott, D.; Galkowski, J.; Wang, L. *Langmuir* **2007**, *23*, 5740–5745.
(4) Pedersen, D. B.; Wang, S.; Liang, S. H. *J. Phys. Chem. C* **2008**, *112*, 8819–8826.
(5) Crooks, R. M.; Zhao, M.; Sun, L. *Acc. Chem. Res.* **2001**, *34*, 181–190.
(6) Balogh, L.; Tomalia, D. A. *J. Am. Chem. Soc.* **1998**, *120*, 7355–7356.
(7) Brelle, M. C.; Torres-Martinez, C. L.; McNulty, J. C. *Pure Appl. Chem.* **2000**, *72*, 101–117.
(8) Shan, J.; Pulkkinen, P.; Vainio, U.; Maijala, J.; Merta, J.; Jiang, H.; Serimaa, R.; Kauppinen, E.; Tenhu, H. *J. Mater. Chem* **2008**, *18*, 3200–3208.
(9) Zhang, H. T.; Wu, G.; Chen, X. H. *Mater. Chem. Phys.* **2006**, *98*, 298–303.
(10) Luechinger, N. A.; Athanassiou, E. K.; Stark, W. J. *Nanotechnology* **2008**, *19*, 445201–445207.
(11) Luechinger, N. A.; Loher, S. L.; Athanassiou, E. K.; Grass, R. N.; Stark, W. J. *Langmuir* **2007**, *23*, 3473–3477.
(12) Brust, M.; Walker, M.; Bethell, D.; Schiffrin, D. J.; Whyman, R. *J. Chem. Soc., Chem. Commun.* **1994**, 801–802.
(13) Sun, X.; Dong, S.; Wang, E. *Mater. Chem. Phys.* **2006**, *96*, 29–33.
(14) Walker, C. H.; John, J. V. S.; Wisian-Neilson, P. *J. Am. Chem. Soc.* **2001**, *123*, 3846–3847.
(15) Wu, C.; Mosher, B.; Zeng, T. *J. Nanopart. Res.* **2006**, *8*, 965–969.
(16) Wang, Y.; Chen, P.; Liu, M. *Nanotechnology* **2006**, *17*, 6000–6006.
(17) Khanna, P.; Gaikwad, S.; Adhyapak, P.; Singh, N.; Marimuthu, R. *Mater. Lett.* **2007**, *61*, 4711–4714.
(18) Kanninen, P.; Johans, C.; Merta, J.; Kontturi, K. *J. Colloid Interface Sci.* **2008**, *318*, 88–95.
(19) Lisiecki, I.; Billoudet, F.; Pileni, M. P. *J. Phys. Chem.* **1996**, *100*, 4160–4166.
(20) Qi, L.; Ma, J.; Shen, J. *J. Colloid Interface Sci.* **1997**, *186*, 498–500.
(21) Song, X.; Sun, S.; Zhang, W.; Yin, Z. *J. Colloid Interface Sci.* **2004**, *273*, 463–469.
(22) Salzemann, C.; Lisiecki, I.; Urban, J.; Pileni, M.-P. *Langmuir* **2004**, *20*, 11772–11777.
(23) Zhu, H.; Zhang, C.; Yin, Y. *Nanotechnology* **2005**, *16*, 3079–3083.
(24) Athawale, A.; Katre, P.; Kumar, M.; Majumdar, M. *Mater. Chem. Phys.* **2005**, *91*, 507–512.
(25) Hirai, H.; Wakabayashi, H.; Komiyama, M. *Bull. Chem. Soc. Jpn.* **1986**, *59*, 367–372.
(26) Guinier, A. *X-ray diffraction. In crystals, imperfect crystals, and amorphous bodies*; Dover Publications, Inc.: New York, 1994.
(27) Sun, J.; Simon, S. L. *Thermochim. Acta* **2007**, *463*, 32–49.
(28) Hong, S. G.; Yeh, C. S. *Polym. Degrad. Stab.* **2004**, *83*, 529–537.
(29) Hong, S. G.; Yeh, C. S. *J. Appl. Polym. Sci.* **2007**, *104*, 442–448.
(30) Yamukyan, M.; Manukyan, K.; Kharatyan, S. *Chem. Eng. J.* **2008**, *137*, 636–642.
(31) Lyubinetsky, I.; Thevuthasan, S.; McCready, D. E.; Baer, D. R. *J. Appl. Phys.* **2003**, *94*, 7926–7928.

AM800177D